DOI: 10.1002/ejic.201100719

A New Family of Homo- and Heterometallic Manganese Complexes at High Oxidation States Derived from the Oxidation of Mn^{II} with Ce^{IV}: Syntheses, Structures, and Magnetic Properties

Cheng-Bing Ma,*[a] Ming-Qiang Hu,[a] Hui Chen,[a] Chang-Neng Chen,*[a] and Qiu-Tian Liu[a]

Keywords: Manganese / Cerium / Cluster compounds / Magnetic properties

A series of homo- and heterometallic manganese(III or IV) clusters, $[Mn_2O_2(pybim)_4](NO_3)_4\cdot 11H_2O$ (**1**; pybim = 2-(2-pyridyl)benzimidazole], $[Mn_3O_4(bipy)_4(H_2O)_2][Ce(NO_3)_5(H_2O)][NO_3]_2\cdot 2H_2O$ (**2**; bipy = 2,2′-bipyridine), $[Mn_2Ce_3O_6(pta)_6(NO_3)_2(dmf)_4]\cdot H_2O$ (**3**; Hpta = *p*-toluic acid), and $[Mn_8CeO_8(pta)_{12}(dmf)_4]$ (**4**), were prepared by the reaction of simple Mn^{2+} salts with $(NH_4)_2[Ce(NO_3)_6]$ under different experimental conditions. The single-crystal X-ray diffraction analyses established that these complexes possess inorganic cores that have various structural topologies, which range from the $[Mn_2O_2]^{4+}$ rhomb, a Mn_3 triangle within $[Mn_3O_4]^{4+}$, and the nonplanar $[Mn_8O_8]^{8+}$ loop that centrally traps a Ce^{4+} ion to the $[Mn_2Ce_3O_6]^{8+}$ cage that contains a Mn_2Ce_3 trigonal bipyramid. The solid-state magnetic susceptibility studies revealed that these four complexes possess distinctly different magnetic properties, namely, both **1** and **2** show strong antiferromagnetic interactions between the Mn^{IV} centers, whereas **3** is weakly antiferromagnetic, and **4**, however, has predominantly ferromagnetic interactions.

Introduction

Discrete, high-valent oxomanganese complexes that contain Mn ions in the +3, +4, or mixed +3/+4 oxidation states have attracted extensive attention over the past few decades.[1–6] Besides the aesthetically pleasing structures they usually possess, the reasons for this attention mainly involve the following aspects: (i) the oxygen-evolving complex (OEC) in the Photosystem II (PSII) is believed to contain a high-valent oxo-bridged tetranuclear Mn cluster that is responsible for the photo-induced oxidation of H_2O to produce O_2, which supports all aerobic life on earth.[2] The structural and the spectroscopic properties, as well as the function, of the OEC are expected to be replicated from the synthetic lower-nuclearity Mn complexes;[3] (ii) the high-valent high nuclearity Mn clusters often have large, and sometimes abnormally large, ground state spin (*S*) values.[4] If these are combined with a large and negative zero-field splitting parameter (*D*) they would exhibit highly unusual magnetic phenomena as has been discovered from the single-molecule magnets (SMMs).[5] This makes these Mn clusters highly attractive as precursors to magnetic materials;[6] and (iii) the high oxidation state Mn oxides and Mn/Ce composite oxides constitute a good catalytic wet-air oxidation system with high activities for the treatment of waste water that contains toxic organic and inorganic pollutants.[7] Thus, as molecular analogues to these oxides, the high-valent Mn or mixed Ce/Mn molecular clusters should have similar oxidative/catalytic properties.

Several pathways have been developed to elevate the oxidation state of the Mn ion during the formation of the manganese complexes, for example, the aerobic oxidation of the Mn^{2+} salts under weakly basic conditions and the comproportionation reaction between the permanganate and the Mn^{2+} salts. Recently Christou et al. employed $(NH_4)_2[Ce(NO_3)_6]$ as an oxidizing agent to react with various Mn-containing precursors and they obtained a series of high oxidation state Mn/Ce clusters, which included Mn^{IV}–Ce^{IV} (Mn^{IV}_2Ce, $Mn^{IV}_6Ce^{IV}$, and $Mn^{IV}_2Ce^{IV}_3$), Mn^{IV}–Ce^{III} ($Mn^{IV}_2Ce^{III}_2$), Mn^{III}–Ce^{IV} ($Mn^{III}_8Ce^{IV}$), and Mn^{III}–$Ce^{III/IV}$ ($Mn^{III}_{10}Ce^{IV}_2Ce^{III}_2$) compounds.[8] We have also prepared several high-valent high nuclearity Mn/Ce complexes with either discrete ($Mn^{III}_8Ce^{IV}$ and $Mn^{IV}_6Ce^{IV}_2$) or polymeric ($[Mn^{IV}_{12}Ce^{IV}_{18}Ce^{III}_4]_n$) structures.[9] It is worth noting that this approach often introduces the oxophilic metal Ce ion into the coordination system, which leads to the richer structural chemistry of the Mn clusters.[8–11]

In the present work we have explored the reaction of simple Mn^{2+} salts and $(NH_4)_2[Ce(NO_3)_6]$, which was used as an oxidant, under a variety of experimental conditions that included a variation in the Ce^{4+}/Mn^{2+} ratios, the acidity of

[a] State Key Laboratory of Structural Chemistry, Fujian Institute of Research on the Structure of Matter, Chinese Academy of Sciences, Fuzhou, Fujian 350002, P. R. China
Fax: +86-591-83792395
E-mail: mcb@fjirsm.ac.cn
ccn@fjirsm.ac.cn

Supporting information for this article is available on the WWW under http://dx.doi.org/10.1002/ejic.201100719.

the medium, and the solvents that were used. A new family of homo- and heterometallic Mn clusters, with various inorganic core topologies that range from the $[Mn_2O_2]^{4+}$ rhomb (**1**), the Mn_3 triangle within $[Mn_3O_4]^{4+}$ (**2**), and the nonplanar $[Mn_8O_8]^{8+}$ loop that centrally traps a Ce^{4+} ion (**3**) to the $[Mn_2Ce_3O_6]^{8+}$ cage that contains a Mn_2Ce_3 trigonal bipyramid (**4**), have been obtained. Their syntheses and structures, as well as their magnetic properties, are discussed.

Results and Discussion

Syntheses

The complexes described in this work were prepared by the oxidation of the Mn^{II} reagent with Ce^{IV} in the presence or absence of the N-donor chelating coligands under various experimental conditions. All of the experiments were found to give high-valent Mn (III or IV) products. Ce^{IV} is an unusually strong, one-electron oxidant, and it is fully capable of oxidizing Mn^{II} to Mn^{III} or Mn^{IV} since the redox pair Ce^{IV}/Ce^{III} possesses a standard electrode potential of 1.72 V that is higher than that of the Mn^{IV}/Mn^{II} pair (1.22 V vs. the standard hydrogen electrode). In fact, some high-valent Mn complexes have been derived previously from the oxidation of the Mn^{2+} salts by Ce^{IV}.[12] The high-, mixed-valent manganese clusters are primarily stabilized with the help of the oxide (O^{2-}) ligands, where the harder oxide ions help to bridge the Mn centers. The presence of the hard O^{2-} ions also favors the incorporation of the hard, high oxidation state Ce^{4+} ion. This facilitates the formation of the mixed-metal Mn/Ce complexes, although the generality of this as a route to the Mn/Ce products, as well as the structural types of the products, and the Mn/Ce ratio in the products, still needs to be investigated further. Some di- and polyimines, for example bipyridyl and terpyridyl, that have been used as ancillary chelating ligands have been demonstrated to play important roles in the formation and stabilization of oxomanganese clusters that contain Mn ions in the +3 and +4 oxidation states.[12,13] The reaction of $Mn(pta)_2{\cdot}2H_2O$ with $(NH_4)_2[Ce(NO_3)_6]$ in the presence of pybim [pybim = 2-(2-pyridyl)-benzimidazole] or bipy (bipy = 2,2′-bipyridine) gave $[Mn_2O_2(pybim)_4](NO_3)_4{\cdot}11H_2O$ (**1**) and $[Mn_3O_4(bpy)_4(H_2O)_2][Ce(NO_3)_5(H_2O)][NO_3]_2{\cdot}2H_2O$ (**2**), respectively. The lower nuclearity of both **1** and **2** is consistent with the presence of the N-donor coligands that function as effective chelates but not as bridging groups. The low pH conditions (the presence of inorganic or organic acid) in both of the reactions excluded the incorporation of Ce^{4+} into the Mn^{4+} coordination sphere (the Ce^{3+} monomer in **2** exists as a counterion outside the Mn cluster). The Mn/Ce ratio of the reactants was not found to strictly affect the formation of the products, but an appropriate increase in the amount of $(NH_4)_2[Ce(NO_3)_6]$ can improve the product yields. Under nearly neutral medium conditions, the reaction between $Mn(pta)_2{\cdot}4H_2O$ (Hpta = p-toluic acid) and $(NH_4)_2[Ce(NO_3)_6]$, without an ancillary N-donor chelating coligand, afforded $[Mn_2Ce_3O_6(pta)_6(NO_3)_2(dmf)_4]{\cdot}H_2O$ (**3**) and $[Mn_8CeO_8(pta)_{12}(dmf)_4]$ (**4**). The common dmf solvent was initially used in order to ensure that the reactant, $Mn(pta)_2{\cdot}4H_2O$, would dissolve but it was found that it also acted as a terminal ligand to both the Mn and Ce centers. The Mn/Ce reagent stoichiometry was not a key factor for the formation of the products, as mentioned above, however, a nearly neutral medium was important for the isolation of **3** and **4** with the Ce^{IV} incorporated. As is the case with almost all of the Mn cluster chemistry, the products **1** to **4** are unlikely to be the only species present. In other words, it is likely that there are several species in each of the reaction equilibria and that the subsequent crystallization that gives the respective single-crystals is strongly dependent on the solubility of the species in a given solution system, which is associated with the solvents used, the acidity of the medium and so on. This means that the successful isolation of **1** to **4** is due to the fact that they crystallize out before the other species in solution get to the saturation point. Interestingly, a closer inspection of the preparation reactions (especially for **3** and **4**) showed that atmospheric oxygen may partly participate in the oxidation of Mn^{II} to Mn^{III}, or even to Mn^{IV}, although the atmospheric oxidation of Mn^{II} to Mn^{IV} is not expected under normal conditions. Thus, the oxide (O^{2-}) ligands in **1** to **4** may originate from multiple sources, namely, from the atmospheric O_2, the water molecule, or their conjunction. Generally, under neutral or weakly basic conditions, atmospheric O_2 has a stronger trend of oxidizing Mn^{II} to the higher-valent species (Mn^{III} or Mn^{IV}). Equations (1), (2), (3), and (4) tentatively describe the formation of complexes **1** to **4**, respectively.

$$2Mn^{2+} + 4(1–x)Ce^{4+} + xO_2 + (13–2x)H_2O + 4pybim + 4NO_3^- \rightarrow [Mn_2O_2(pybim)_4](NO_3)_4{\cdot}11H_2O + 4(1–x)H^+ + 4(1–x)Ce^{3+} \quad (1)$$

$$3Mn^{2+} + (6–4x)Ce^{4+} + xO_2 + (9–2x)H_2O + 4bipy + 7NO_3^- \rightarrow [Mn_3O_4(bpy)_4(H_2O)_2][Ce(NO_3)_5(H_2O)][NO_3]_2{\cdot}2H_2O + (5–4x)Ce^{3+} + 4(2–x)H^+ \quad (2)$$

$$2Mn^{2+} + (7–4x)Ce^{4+} + xO_2 + 4dmf + 6pta^- + (7–2x)H_2O + 2NO_3^- \rightarrow [Mn_2Ce_3O_6(pta)_6(NO_3)_2(dmf)_4]{\cdot}H_2O + 4(1–x)Ce^{3+} + 4(3–x)H^+ \quad (3)$$

$$8Mn^{2+} + (9–4x)Ce^{4+} + xO_2 + 4dmf + 12pta^- + 2(4–x)H_2O \rightarrow [Mn_8CeO_8(pta)_{12}(dmf)_4] + 4(4–x)H^+ + 4(2–x)Ce^{3+} \quad (4)$$

O2 is used to balance Equations (1) to (4), which reflects the participation of O2 in the oxidizing of Mn(II) to Mn(III) or Mn(IV), and the coefficient x varies between 0 and 1.

Description of the Structures of the Complexes 1 to 4

The structure of complex **1** consists of one discrete $[Mn_2O_2(pybim)_4]^{4+}$ cation, four nitrate anions, and eleven water molecules of crystallization. The bond lengths and bond angles that pertain to the inner coordination of Mn are listed in Tables 1 and S1, respectively, and the structural drawing of the cation is shown in Figure 1. The cation is situated on a twofold axis of symmetry, which passes

through the Mn1–Mn2 bond, and hence half of the cation is crystallographically independent. The two manganese centers in the cationic cluster are bridged by two O^{2-} ions to yield a planar Mn_2O_2 rhombic core in which the Mn···Mn distance is 2.7161(16) Å, which is similar to that found in the $[Mn_2O_2]^{4+}$ cores of the phenanthroline or picolinic acid complexes,[14] and therefore indicates no significant metal–metal bond. The two chelating pybim ligands complete the roughly octahedral coordination geometry around the Mn center with *cis* angles that range from 78.97(12) to 100.90(11)°. The average Mnl–N distance [2.023(3) Å] is very close to the average Mn2–N distance [2.030(3) Å], which suggests that the coordination geometries of the two Mn atoms are almost identical. The lack of evidence for the Jahn–Teller elongation, as well as the bond valence sum calculations (Table S2), confirm that both of the Mn atoms are in the +4 oxidation state. It is worth noting that the Mn···Mn span of 2.7161(16) Å may be used to support the existence of a $[Mn_2(\mu\text{-}O)_2]$ fragment in the OEC of PSII since the crystal structure data on this enzyme at 1.9 Å resolution has indicated that a short (ca. 2.8–3.0 Å) Mn···Mn separation is present.[2f]

Table 1. The selected bond lengths [Å] for **1**.

Mn1–O1	1.794(2)	Mn2–O1	1.803(2)
Mn1–N2	1.963(3)	Mn2–N5	1.974(3)
Mn1–N1	2.083(3)	Mn2–N4	2.086(3)
Mn1···Mn2	2.7161(16)		

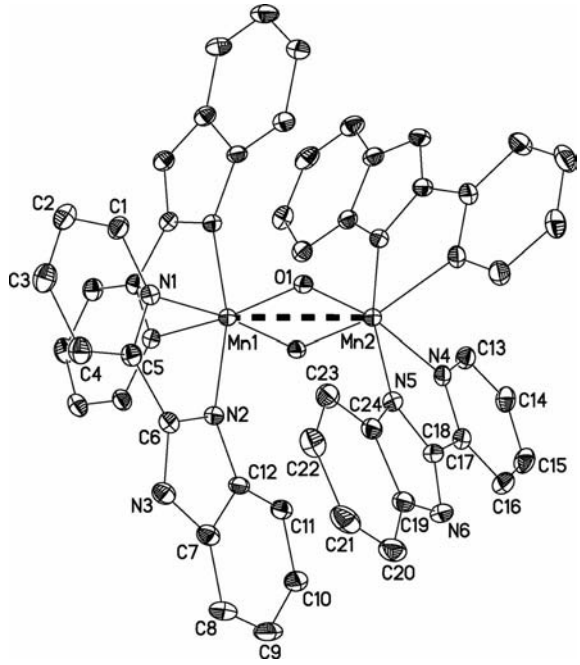

Figure 1. A structural view of the cluster cation in **1** with the selected atom labeling scheme ellipsoids at 30% probability. All of the hydrogen atoms have been omitted for clarity.

Abundant hydrogen bonds are present within the crystal lattice of **1** (Table S3). Besides the two short N–H···O hydrogen bonds [N···O 2.680(4) and 2.659(5) Å] that formed between the imidazole N atoms of the pybim ligands and the nitrate/water O atoms, the water molecules and the nitrate anions trigger a complicated hydrogen bond network where the O···O distances are in the range of 2.814(12) to 2.909(10) Å. The cationic clusters are associated together by means of these hydrogen bonding interactions to yield an ordered 3D supramolecular array (Figure S1).

Complex **2** crystallizes in the monoclinic, non-centric space group *C*/*c* with the absolute structure Flack parameter refined to 0.061(15). The structure consists of one trinuclear cationic cluster $[Mn_3O_4(bipy)_4(H_2O)_2]^{4+}$ with one monomeric $[Ce(NO_3)_5(H_2O)]^{2-}$ anion and two nitrates as the counterions, and two water molecules of crystallization. All of the components are in general crystallographic positions. As shown in Figure 2, the cluster cation contains a core of $[Mn_3O_4]$, in which three Mn atoms reside on the vertices of a nearly isosceles triangle. One of the three Mn atoms (Mn3) is linked to the other two Mn atoms (Mn1 and Mn2) by means of two single oxo-bridges (O3 and O4). The Mn1···Mn3 and Mn2···Mn3 distances are nearly equal [3.2590(14) and 3.2531(14) Å, respectively]. Mn1 and Mn2 are linked to each other by the di-μ-oxo bridge (O1 and O2), which affords a slightly shorter Mn···Mn distance [2.6704(14) Å] than that found in **1** [2.7161(16) Å]. The two single μ-oxo bridges (O3 and O4) are nearly coplanar with the three Mn atoms, while the doubly oxo-bridged $[Mn_2O_2]$ segment exhibits a slight fold along the Mn1–Mn2 bond with a small dihedral angle of 16.2°. The two motifs (Mn1/Mn2/Mn3/O3/O4 and Mn1/Mn2/O1/O2) are nearly perpendicular to each other. The Mn coordinations are octahedrally completed either by four bipy N atoms (for Mn3) or by two bipy N atoms and one water O atom (for both Mn1 and Mn2).

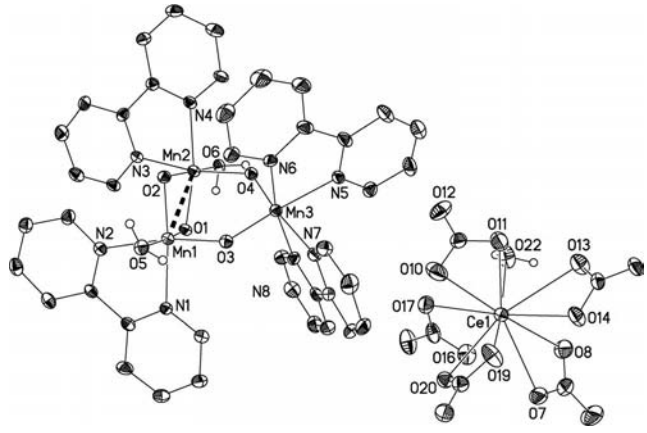

Figure 2. A structural view of $[Mn_3O_4(bipy)_4(H_2O)_2][Ce(NO_3)_5(H_2O)]$ in **2** with the selected atom labeling scheme ellipsoids at 30% probability. The hydrogen atoms, except for those on the coordinated water molecules, have been omitted for clarity.

The average Mn–N and Mn–O_{oxo} distances [2.057(6) and 1.803(5) Å, respectively], as well as the bond valence sum calculations (Table S2, Supporting Information), confirm that the cationic cluster in **2** contains three Mn^{IV} ions. As listed in Tables 2 and S4, the structural parameters that relate to the $[Mn_3O_4]$ core are comparable to the analogous complex cations, namely $[Mn_3O_4(bipy)_4Cl_2]^{2+}$ and

$[Mn_3O_4(phen)_4(H_2O)_2]^{4+}$.[12b,15] However, the Mn–O_{aqua} distances [1.986(6) and 2.039(6) Å] are shorter than those that have been reported previously for any of the analogs,[13a,15] even though the coordinated water molecules in the present cation extensively engage in hydrogen bonding with the lattice water molecules and nitrates [O_{aqua}···O_{aqua}/nitrate distances are in the range of 2.563(2)–2.878(2) Å]. It has been postulated that the water that is directly bound to a high-valent Mn^{IV} center with strong hydrogen bonds is the source of the O_2 that evolves during photosynthesis[2f,3e,16] since the hydrogen bonds render the oxygen of the water molecule more electron-rich.[17]

Table 2. The selected bond lengths [Å] for **2**.

Mn1–O1	1.806(5)	Mn2–N4	2.070(6)
Mn1–O2	1.807(5)	Mn3–O3	1.758(5)
Mn1–O3	1.827(5)	Mn3–O4	1.779(5)
Mn1–O5	1.986(6)	Mn3–N6	2.006(6)
Mn1–N1	2.071(6)	Mn3–N8	2.011(6)
Mn1–N2	2.076(6)	Mn3–N7	2.077(6)
Mn2–O1	1.803(5)	Mn3–N5	2.092(6)
Mn2–O2	1.811(5)	Mn1···Mn2	2.6704(14)
Mn2–O4	1.835(5)	Mn1···Mn3	3.2590(14)
Mn2–O6	2.039(6)	Mn2···Mn3	3.2531(14)
Mn2–N3	2.058(6)		

On the basis of the electron-neutrality consideration for the whole complex **2**, the Ce atom in the $[Ce(NO_3)_5(H_2O)]^{2-}$ counterion is in the +3 oxidation state. The Ce^{III} center, which is in a distorted monocapped pentagonal prismatic geometry, is eleven-coordinated by five bidentate chelating nitrato ligands and one water molecule and has Ce–O bond lengths in the range of 2.494(9) to 2.731(8) Å (Table S5). The $[Ce(NO_3)_5(H_2O)]^{2-}$ anion is associated with the complex cation through extensive hydrogen bonding interactions, which appear to involve all of the components since too many donor/acceptor groups are present in the structure (Table S6).

Complex **3** is a neutral discrete pentanuclear heterometal cluster. There was no evidence of Jahn–Teller elongation and the charge considerations, as well as the bond valence sum calculations (Table S2), established that a $Mn^{IV}{}_2Ce^{IV}{}_3$ situation exists in complex **3**. The selected bond lengths and bond angles are listed in Tables 3 and S7, respectively. The whole molecule lies on a general crystallographic position. As shown in Figures 3 and 4, the structure of the cluster contains a cage-like core of $[Mn_2Ce_3O_6]$, in which five metal atoms display a trigonal bipyramidal arrangement with three Ce atoms that define the triangle equatorial plane [Ce···Ce 3.694(3)–3.737(3) Å]. The Ce_3 triangle is attached to two Mn atoms [Mn···Mn 4.798(3) Å] above and below the triangle plane by means of six μ_3-O ions. The six μ_3-O ions are each located above the six triangle faces of the trigonal bipyramid, which thus completes a cage-like $[Mn_2Ce_3O_6]$ core. Each of the Mn/Ce ion pairs is additionally bridged by one pta^- ligand [Mn···Ce 3.1857(9)–3.2458(9) Å]. The two Mn atoms are thus normally six-coordinate. The peripheral ligands around the three Ce atoms also contain four terminal dmf molecules and two chelating nitrate anions, which affords two kinds of coordination en-

Table 3. The selected bond lengths [Å] for **3**.

Ce1–O18	2.290(3)	Ce3–O17	2.271(3)
Ce1–O16	2.301(3)	Ce3–O18	2.296(3)
Ce1–O15	2.320(3)	Ce3–O13	2.305(3)
Ce1–O17	2.336(3)	Ce3–O12	2.375(3)
Ce1–O4	2.382(3)	Ce3–O26	2.394(4)
Ce1–O7	2.397(3)	Ce3–O1	2.405(3)
Ce1–O25	2.401(3)	Ce3–O28	2.444(4)
Ce1–O20	2.500(4)	Mn1–O17	1.827(3)
Ce1–O19	2.631(4)	Mn1–O15	1.829(3)
Ce2–O13	2.293(3)	Mn1–O13	1.833(3)
Ce2–O16	2.308(3)	Mn1–O5	1.976(3)
Ce2–O15	2.316(3)	Mn1–O3	1.993(3)
Ce2–O14	2.316(3)	Mn1–O2	1.998(3)
Ce2–O9	2.399(3)	Mn2–O16	1.827(3)
Ce2–O27	2.418(4)	Mn2–O14	1.833(3)
Ce2–O6	2.432(3)	Mn2–O18	1.836(3)
Ce2–O22	2.489(4)	Mn2–O8	1.966(3)
Ce2–O23	2.633(4)	Mn2–O10	1.970(3)
Ce3–O14	2.264(3)	Mn2–O11	1.988(3)

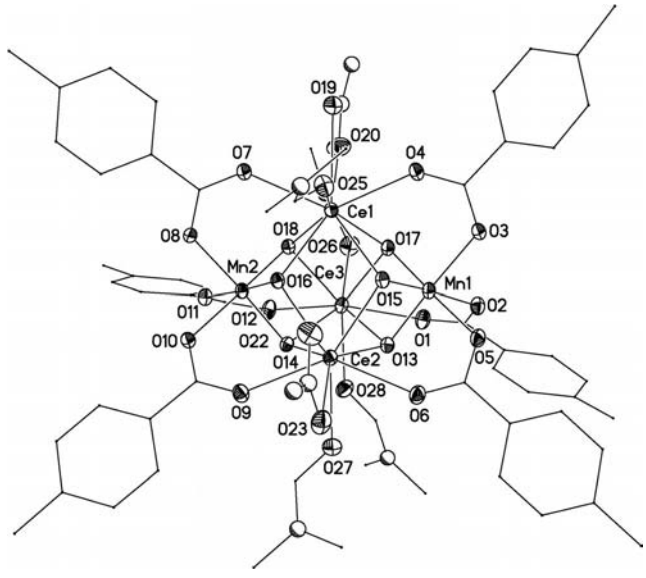

Figure 3. A structural view of **3** with the selected atomic labeling scheme ellipsoids at 30% probability. For clarity, all of the carbon atoms are shown as small spheres of reduced radii and the uncoordinated O/N atoms of both dmf and NO_3^- are shown as small spheres of arbitrary radii.

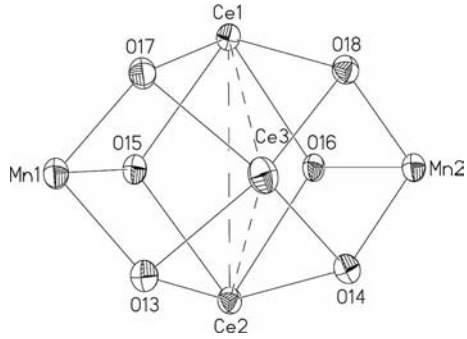

Figure 4. The $[Mn_2Ce_3O_6]^{8+}$ core in **3**, which shows the cage-like structure.

vironments around the three Ce atoms. One of the Ce atoms (Ce3) is eight-coordinate with a distorted dodecahedral geometry that is completed by two terminal dmf molecules, whereas the other two Ce atoms (Ce1 and Ce2) exhibit distorted tricapped trigonal prism or heptagonal bipyramid 9-coordination geometries, where each Ce is peripherally ligated by one dmf molecule and one chelating nitrate anion.

Table 4. The selected bond lengths [Å] for **4**.

Ce1–O8	2.305(3)	Mn1–O3	2.345(4)
Ce1–O7	2.381(4)	Mn2–O8B	1.854(4)
Mn1–O8	1.853(4)	Mn2–O7	1.867(4)
Mn1–O7	1.869(4)	Mn2–O6	1.983(4)
Mn1–O5	1.959(4)	Mn2–O2B	1.979(4)
Mn1–O1	1.961(4)	Mn2–O9	2.220(5)
Mn1–O4A[a]	2.145(4)	Mn2–O3	2.332(4)

[a] Symmetry codes, A: $-y + 3/2$, x, $-z + 1/2$; B: y, $-x + 3/2$, $-z + 1/2$.

Complex **4** is made up of discrete neutral $[Mn_8CeO_8(pta)_{12}(dmf)_4]$ clusters and crystallizes in the tetragonal space group $P4_2/n$. The selected bond lengths and bond angles are listed in Tables 4 and S8, respectively. The whole molecule lies on a crystallographic fourfold axis of symmetry that passes through the central Ce atom with the asymmetric unit thus containing a quarter of the cluster. As shown in Figures 5 and 6, the structure contains a cluster core of $[Mn_8CeO_8]$, in which the eight Mn atoms and the eight O atoms form a nonplanar $[Mn_8O_8]$ loop with the Mn and O atoms arranged alternately. The adjacent Mn···Mn distances of the loop are 3.0259(12) and 3.2376(12) Å. The $[Mn_8O_8]$ ring is further attached to the central Ce atom by means of eight O^{2-} ions, which each act as a μ_3-linker. The peripheral eight $\mu_{1,3}$- and four $\mu_{1,1,3}$-bridging pta^- ligands and the four terminal dmf molecules complete the near-octahedral coordination around each of the Mn atoms. The charge consideration and the bond valence sum calculations (Table S2), as well as the Jahn–Teller effect established that all of the Mn atoms are in the +3 oxidation state and that

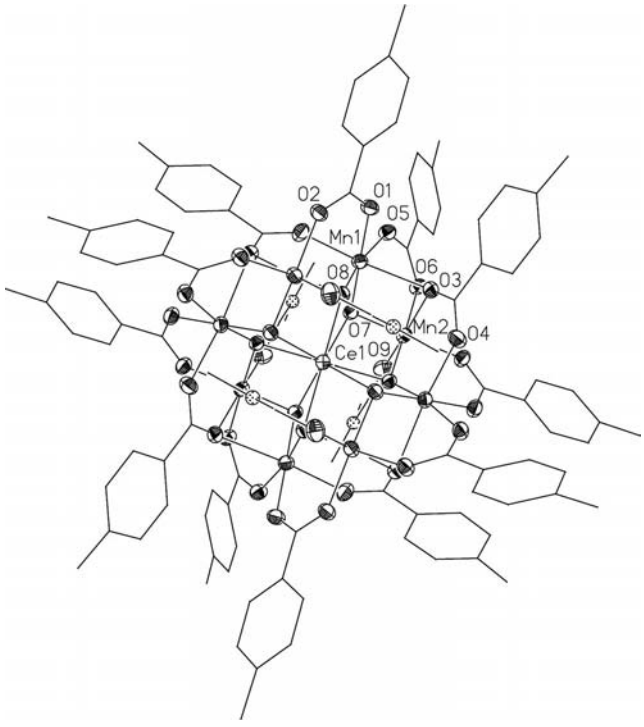

Figure 5. A structural view of **4** with the selected atomic labeling scheme ellipsoids at 30% probability. All of the carbon atoms are shown as small spheres of reduced radii for clarity.

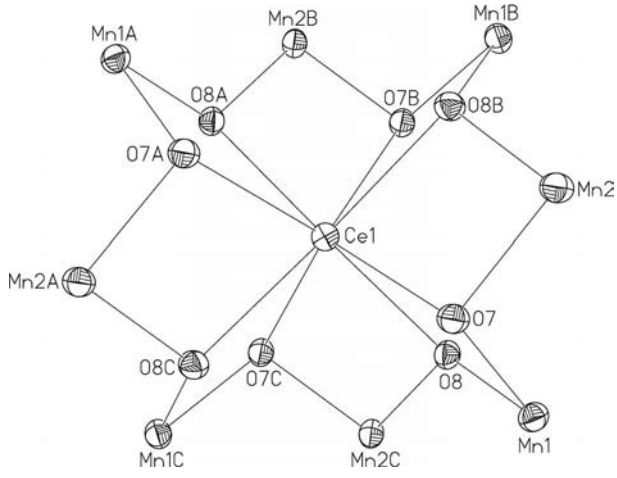

Figure 6. The core of $[Mn_8CeO_8]^{12+}$ in **4**, which shows the Ce-trapped Mn_8O_8 loop structure.

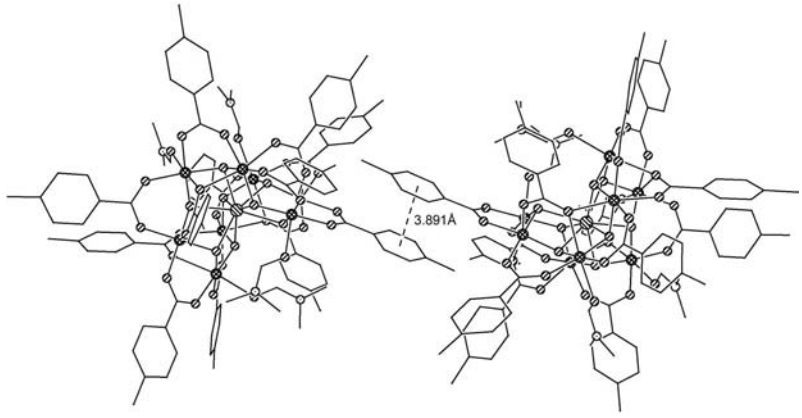

Figure 7. A view of the π–π-interaction between a pair of clusters in **4**.

the central Ce atom is in the +4 oxidation state. The eight Mn^{III} atoms exhibit the expected Jahn–Teller distortion for a high-spin Mn^{III} (d^4) in an octahedral geometry with sixteen oxygen atoms (O3, O4, and O9, and their symmetry-related equivalents) from the $\mu_{1,1,3}$-pta$^-$ ligands and the dmf molecules, which are located at the elongated axial positions [Mn–O 2.145(4)–2.332(4) Å]. Presumably it is this axial elongation, which is associated with the Mn^{III} (d^4) Jahn–Teller effect, that makes the occasionally strict orthogonality of the magnetic orbitals of the interacting Mn^{III} ions,[18] which thus leads to the ferromagnetically coupled Mn^{III}–Mn^{III} species (vide infra). The central Ce^{IV} atom, which is in a distorted trigonal dodecahedral geometry, is eightfold coordinated to the O^{2-} ions and the Ce–O bond lengths range from 2.305(3) to 2.381(4) Å. Significant stacking interactions that involve the pta$^-$ ligands from the inversion-related clusters, which have a centroid–centroid distance of 3.891 Å between the benzene rings (C17–C22) at (x, y, z) and ($1 - x$, $2 - y$, $-z$), were observed (Figure 7). Each cluster unit thus functions as a 4-connected node to π–π-interact with four other adjacent units, which results in a three-dimensional supramolecular pack mode for the whole solid structure (Figure S2).

Magnetic Properties of Complexes 1 to 4

The temperature (T) dependence of the molar magnetic susceptibility (χ_M) complex **1** is shown in Figure 8 in the form of a $\chi_M T$ versus T plot. The product $\chi_M T$ of 0.79 $cm^3 K mol^{-1}$ at room temperature is much smaller than the spin-only value (3.75 $cm^3 K mol^{-1}$) that is expected for two noninteracting Mn^{IV} centers, and it monotonically declines to 0.19 $cm^3 K mol^{-1}$ at approximately 50 K before remaining constant down to 2 K. This is behavior is typical of a strong antiferromagnetic couple between the paramagnetic centers. The experimental data were fitted by employing Equation (5) that was derived from an isotropic spin-exchange Hamiltonian, $\hat{H} = -2J\hat{S}_1\hat{S}_2$ ($S_1 = S_2 = 3/2$), and the Van Vleck equation.[19] The best least-squares fit results were obtained in the full temperature range with parameters $J = -143.38\ cm^{-1}$, TIP = $400 \times 10^{-6}\ cm^3 K mol^{-1}$ (fixed), $g = 2.00$ (fixed), $P = 0.047$, and $R = 7.58 \times 10^{-4}$, where TIP is the temperature-independent paramagnetism, P is the percentage of a paramagnetic impurity that was assumed to be a mononuclear Mn^{IV} species, and R is the agreement factor. The relatively large coupling constant ($-143.38\ cm^{-1}$), which falls in the range of –79 to $-188\ cm^{-1}$,[20] suggested a strong magnetic exchange interaction between the two Mn^{IV} centers that are closely linked (ca. 2.7 Å) through the di-μ-oxo bridge.

$$\chi_M = \frac{2Ng^2\beta^2}{kT}\left[\frac{\exp(\frac{2J}{kT}) + 5\exp(\frac{6J}{kT}) + 14\exp(\frac{12J}{kT})}{1 + 3\exp(\frac{2J}{kT}) + 5\exp(\frac{6J}{kT}) + 7\exp(\frac{12J}{kT})}\right] \quad (5)$$

As shown in Figure 9, the product $\chi_M T$ of complex **2** at room temperature is equal to 2.69 $cm^3 K mol^{-1}$, which is much lower than the expected spin-only value (5.63 $cm^3 K mol^{-1}$) for the sum of three isolated Mn^{IV} ions and one Ce^{III} ion, and decreases gradually to 0.64 $cm^3 K mol^{-1}$ at 2 K. This behavior is characteristic of antiferromagnetic interactions between the paramagnetic centers. On the basis of the structure of **2**, the experimental data were fitted to a simplified isotropic exchange model that is based on three Mn^{IV} ($S_1 = S_2 = S_3 = 3/2$) centers that are arranged in an isosceles triangle where the assumption is that Mn1 and Mn2 are equidistant from Mn3 and where an isolated outer Ce^{III} ion is included. The spin Hamiltonian is thus written as $\hat{H} = -2J_1\hat{S}_1\hat{S}_2 - 2J_2(\hat{S}_1\hat{S}_3 + \hat{S}_2\hat{S}_3) + \hat{S}_{Ce}$, where the two distinct coupling parameters J_1 and J_2 represent the interactions across the di-μ-oxo bridge and across the mono-μ-oxo bridges, respectively, and the third term on the right-hand side accounts for the isolated Ce^{III} center. Equation (6) describes the molar magnetic susceptibility (χ_M) as a function of temperature and was derived from a combination of a Van Vleck equation for the isosceles triangular Mn^{IV} trimer and a Curie–Weiss formula for the single Ce^{III} ion.[19,21]

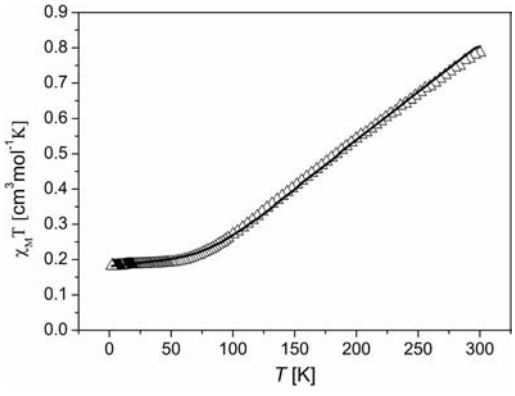

Figure 8. Plots of the product ($\chi_M T$) vs. temperature (T) for **1**; χ_M is the molar magnetic susceptibility and the solid line represents the calculated value.

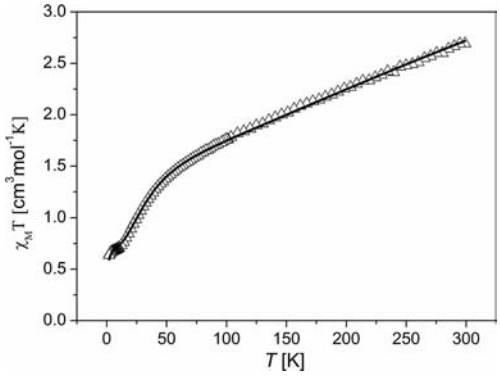

Figure 9. Plots of the product ($\chi_M T$) vs. temperature (T) for **2**; χ_M is the molar magnetic susceptibility and the solid line represents the calculated value.

$$\chi_M = \chi_M^{Mn} + \chi_M^{Ce} \quad (6)$$

where $\chi_M^{Mn} = \frac{Ng_{Mn}^2\beta^2}{3kT}\frac{A}{B}$

$$A = \frac{990}{4}\exp(\frac{12J_1+12J_2}{kT}) + \frac{504}{4}\exp(\frac{12J_1+3J_2}{kT}) + \frac{210}{4}\exp(\frac{12J_1-4J_2}{kT}) + \frac{60}{4}\exp(\frac{12J_1-9J_2}{kT})$$
$$+ \frac{210}{4}\exp(\frac{6J_1+2J_2}{kT}) + \frac{504}{4}\exp(\frac{6J_1+9J_2}{kT}) + \frac{60}{4}\exp(\frac{6J_1-3J_2}{kT}) + \frac{6}{4}\exp(\frac{6J_1-6J_2}{kT})$$
$$+ \frac{210}{4}\exp(\frac{2J_1+6J_2}{kT}) + \frac{60}{4}\exp(\frac{2J_1+J_2}{kT}) + \frac{6}{4}\exp(\frac{2J_1-2J_2}{kT}) + \frac{60}{4}\exp(\frac{3J_2}{kT})$$

$$B = 10\exp(\frac{12J_1+12J_2}{kT}) + 8\exp(\frac{12J_1+3J_2}{kT}) + 6\exp(\frac{12J_1-4J_2}{kT}) + 4\exp(\frac{12J_1-9J_2}{kT}) + 6\exp(\frac{6J_1+2J_2}{kT})$$
$$+ 8\exp(\frac{6J_1+9J_2}{kT}) + 4\exp(\frac{6J_1-3J_2}{kT}) + 2\exp(\frac{6J_1-6J_2}{kT}) + 6\exp(\frac{2J_1+6J_2}{kT}) + 4\exp(\frac{2J_1+J_2}{kT})$$
$$+ 2\exp(\frac{2J_1-2J_2}{kT}) + 4\exp(\frac{3J_2}{kT})$$

Fairly good least-squares fit results were obtained in the full temperature range with the parameters J_1 = –69.21 cm^{-1}, J_2 = –36.16 cm^{-1}, g_{Mn} = 2.04, g_{Ce} = 2.06, the Weiss constant θ = –1.91 K, and $R = 1.87 \times 10^{-3}$. In practice, the magnetic properties of the rare-earth-containing complexes may be rather complicated because they are affected by numerous factors that include the contribution of the orbital momentum, the spin-orbit coupling effect, the thermal population of the excited states, and so on, thus, the precise interpretation of the experimental data remains difficult in most cases, which is in contrast to the 3*d* transition metal species. The ^2F ground term of the Ce^{III} ion is split by the spin-orbit coupling into two states, namely, the ground state $^2F_{5/2}$ and the excited state $^2F_{7/2}$. The two states are well separated in energy (above 2200 cm^{-1}) from each other, such that only the ground state is thermally populated at room temperature and below.[21] In the free-ion approximation, the molar magnetic susceptibility for the Ce^{III} monomer is thus expressed in the form of a Curie-like formula [Equation (7)] as

$$\chi_M^{Ce} = \frac{Ng_J^2\beta^2}{3k(T-\theta)}J(J+1) \quad (7)$$

where J is the quantum number that is associated with the total magnetic momentum J defined as $J = L + S$, and g_J is the Zeeman factor.[21,22] In the combination of Equations (6) and (7) an alternative fit was carried out where the contribution of the orbital momentum of the Ce^{III} ion was considered. The least-squares fit results were obtained with J_1 = –66.35 cm^{-1}, J_2 = –35.13 cm^{-1}, g_{Ce} = 0.64, the Weiss constant θ = –2.39 K, and $R = 3.35 \times 10^{-3}$, with g_{Mn} fixed at 2.00, in the full temperature range. Although the latter fit was also mathematically fairly good, the g_{Ce} value of 0.64 is smaller than the expected value (g_J = 6/7) for the ground state Ce^{III} ion ($^2F_{5/2}$). The attempts to elevate the g_{Ce} value during the data fitting resulted in an increase in the agreement factor, R, which indicates worse fitting results. The deviation is probably the consequence of the ligand field splitting of the ground state $^2F_{5/2}$ into three Kramers doublets. Both of the fittings gave almost coincident coupling parameters, J_1 and J_2, within the [Mn_3O_4] core, which unequivocally shows that the exchange interaction of J_1 across the di-μ-oxo bridge is larger than that of J_2 across the mono-μ-oxo bridges. However, the J_1 value is much smaller than that which was found in **1** (–143.38 cm^{-1}) where the exchange interaction of J_1 was similarly mediated by the di-μ-oxo bridge. This may be due to the difference in the overlap of the magnetic orbitals of two interacting metal centers as a result of different crystal symmetries.

For complex **3**, as shown in Figure 10, the $\chi_M T$ value of 3.59 cm^3 K mol^{-1} at room temperature is slightly lower than the spin-only value (3.75 cm^3 K mol^{-1}) that is expected for two isolated Mn^{IV} ions (the Ce^{IV} ion, f^0 configuration is diamagnetic) and it remains essentially constant before a small drop that occurs at approximately 10 K. This behavior suggests that there are overall weak antiferromagnetic interactions within the complex. The experimental data were fitted by employing the same isotropic spin Hamiltonian $\hat{H} = -2J\hat{S}_1\hat{S}_2$ ($S_1 = S_2 = 3/2$) as was used for **1**. The best least-squares fit results were obtained in the full temperature range with parameters J = –0.46 cm^{-1}, TIP =

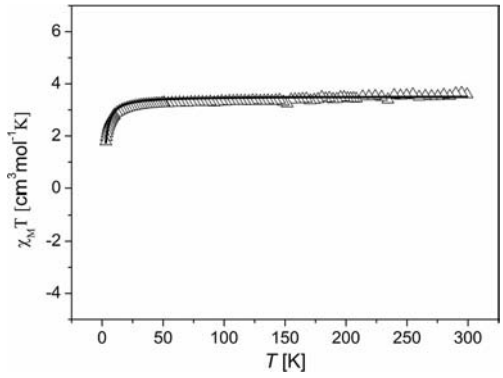

Figure 10. Plots of the product ($\chi_M T$) vs. temperature (T) for **3**; χ_M is the molar magnetic susceptibility and the solid line represents the calculated value.

500×10^{-6} cm^3 K mol^{-1} (fixed), g = 1.93, P = 0.039, and R = 4.21×10^{-4}. The small J value indicates a very weak exchange coupling in **3**, which is expected for the two 4.798(2) Å-separated Mn^{IV} ions that interact through the long four-bond superexchange pathways.

For complex **4**, as shown in Figure 11, the $\chi_M T$ value of 22.65 cm^3 K mol^{-1} at room temperature is close to the value of 24 cm^3 K mol^{-1} for eight noninteracting Mn^{III} centers (Ce^{IV} is diamagnetic) and increases steadily to 28.91 cm^3 K mol^{-1} at approximately 50 K before rapidly decreasing to 6.22 cm^3 K mol^{-1} at 2 K. This behavior suggests that predominantly ferromagnetic interactions exist within the complex and a relatively large spin ground state is present as judged from the maximum value of 28.91 cm^3 K mol^{-1}. The $\chi_M T$ drop in the low-temperature region was attributed to the Zeeman effects, zero-field splitting, and/or weak intermolecular interactions. The eight Mn^{III} centers will give total S values in the range of 0 to 16. It was not easy to calculate the various Mn_2 pairwise exchange parameters within **4** owing to the size and low symmetry of the molecule. In order to determine the nature of the ground state, the magnetization (M) data were collected in the 2.0 to 10.0 K and 5 to 40 kG ranges and plots of $M/N\mu_B$ versus H/T are shown in Figure 12. By assuming that only the ground state is populated, the data were fitted

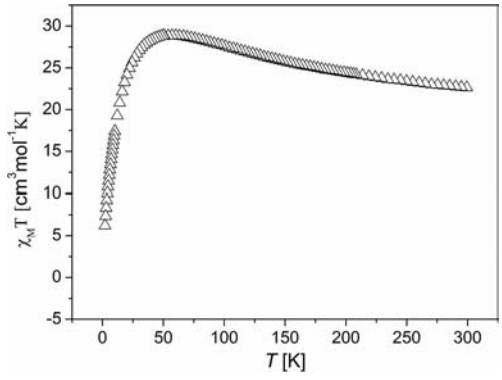

Figure 11. Plot of the product ($\chi_M T$) vs. temperature (T) for **4**; χ_M is the molar magnetic susceptibility.

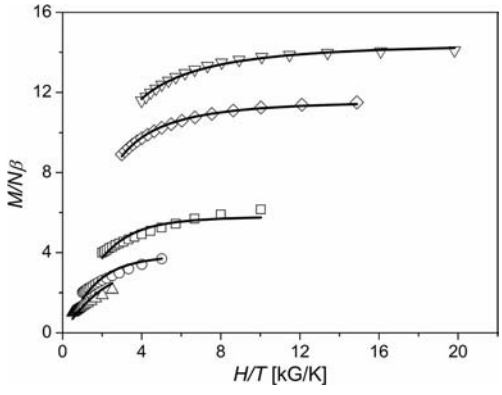

Figure 12. Plots of reduced magnetization ($M/N\mu_B$) vs. H/T for **4** at 40 (▽), 30 (◇), 20 (□), 10 (○), and 5 (△) kG. The solid lines represent the fits to the data as was calculated by using Anisofit2.0.

with Anisofit2.0,[23] by using S = 7 by diagonalization of the spin Hamiltonian matrix including axial zero-field splitting ($D\hat{S}_z^2$) and Zeeman interactions. The fitting results (the solid lines in Figure 12) were obtained with parameters D = –0.0058 cm^{-1} and g = 1.87. An alternative fit with S = 8 or 6 has been done but no improved results were obtained. The ground state of S = 7 is significantly lower than that found in $[Mn_8CeO_8(O_2CMe)_{12}(H_2O)_4]$ (S = 16) but is larger than that found in the previously reported $[Mn_8CeO_8(O_2CMe)_{12}(py)_4]$ (S = 4 or 5),[24] which is probably as a result of the differences in the crystal symmetry.

Conclusions

The reaction of the Mn^{2+} salts with the oxidizing agent $(NH_4)_2[Ce(NO_3)_6]$ was explored in order to investigate the effect of a variety of conditions, which included the Mn^{2+}/Ce^{4+} ratio, the acidity of the medium, the solvents used, and the addition of chelating coligands, on the formation of the high oxidation state Mn complexes. Four homo- and heterometallic complexes with various inorganic core topologies, which included the $[Mn_2O_2]^{4+}$ rhomb, the Mn_3 triangle within $[Mn_3O_4]^{4+}$, the nonplanar $[Mn_8O_8]^{8+}$ loop with the centrally trapped Ce^{4+} ion, and the $[Mn_2Ce_3O_6]$ cage that contains a Mn_2Ce_3 trigonal bipyramid, were prepared. It became apparent that Ce^{IV} is a suitable oxidant for oxidizing Mn^{II} to Mn^{III} or Mn^{IV}. There is a strong tendency for both metals to be incorporated into one coordination environment to yield mixed-metal clusters at high oxidation states since the hard O^{2-} ion favors both bridging/binding to and stabilizing of the hard metal ions, such as Mn^{III}, Mn^{IV}, and Ce^{IV}. The magnetic studies established that the coupling interactions between the Mn atoms in complexes **1** to **3** are all antiferromagnetic, as is expected for the Mn^{IV} spin carriers, and that the differences in the interaction magnitudes can be rationalized on the basis of the structural parameters. Complex **4** displays ferromagnetic interactions among the eight Mn^{III} atoms, which relates to the high-spin Mn^{III} (d^4) configuration with a Jahn–Teller distortion. This work further demonstrates a suitable approach to the high-valent oxomanganese complexes by means of the Ce^{IV} oxidation of the Mn^{II} salts. The resultant heterometallic Ce/Mn products are a rich source of new structural types and are an important addition to the Mn chemistry, although the general rules still need to be investigated further in future studies.

Experimental Section

General Remarks: All of the manipulations were performed under aerobic conditions and all of the chemicals were of reagent grade and were used as received. $Mn(pta)_2{\cdot}2H_2O$ was prepared from manganese(II) chloride tetrahydrate, *p*-toluic acid, and sodium hydroxide in a 1:2:2 molar ratio in water and the composition was confirmed by elemental analysis. The elemental analyses were performed with a Vario EL-III element analyzer. The IR spectra (KBr pellets, 4000–400 cm^{-1}) were recorded with a Magna-75-FT-IR spectrophotometer. The variable-temperature magnetic suscep-

tibilities were measured over a temperature range of 2 to 300 K on crystalline samples with a Quantum Design MPMS-XL SQUID magnetometer in an applied field of 1 kG (for complex **1**) or 10 kG (for complexes **2**–**4**). Background corrections for the sample holder and diamagnetic corrections that were estimated with Pascal's constants for all of the complexes were applied.

$[Mn_2O_2(pybim)_4](NO_3)_4\cdot 11H_2O$ (1): Solid 2-(2-pyridyl)benzimidazole (0.78 g, 4 mmol) was added to a stirred red solution of $Mn(pta)_2\cdot 2H_2O$ (0.72 g, 2 mmol) in EtOH/dmf(20 mL, v/v 3:1). The solution was stirred for 0.5 h and yielded a pale yellow slurry. H_2O/MeCOOH (20 mL, v/v 3:1) was added to the mixture, which gave a clear yellow solution. Solid $(NH_4)_2[Ce(NO_3)_6]$ (2.74 g, 5 mmol) was then added in small batches to the above solution over a period of 0.5 h and resulted in a clear dark solution. The solution was stirred for an additional 6 h, then filtered and the filtrate was left undisturbed for several weeks at room temperature, during which time the black hollow column crystals of **1** were deposited, collected by filtration, washed with a small amount of EtOH, and dried in air; yield 0.32 g (23% based on Mn). $C_{48}H_{58}Mn_2N_{16}O_{25}$ (1368.98): calcd. C 42.11, H 4.27, N 16.37; found C 42.24, H 4.33, N 16.26. Selected IR data (KBr): $\tilde{\nu}$ = 3434 (s, br), 1609 (s), 1481 (s), 1457 (s), 1385 (vs), 1324 (s), 1303 (s), 1150 (m), 1116 (m), 1061 (w), 1019 (w), 1007 (w), 992 (m), 975 (m), 908 (w), 820 (s), 790 (m), 752 (s), 693 (s), 655 (m), 582 (m), 501 (w), 435 (m), 417 (w) cm^{-1}.

$[Mn_3O_4(bipy)_4(H_2O)_2][Ce(NO_3)_5(H_2O)][NO_3]_2\cdot 2H_2O$ (2): Solid 2,2′-bipyridine (0.62 g, 4 mmol) was added to a stirred red solution of $Mn(pta)_2\cdot 2H_2O$ (1.08 g, 3 mmol) in EtOH/dmf(35 mL, v/v 6:1), which resulted in a yellow suspension. Concentrated nitric acid (63%, 5 mL) was then added and resulted in a clear solution. Solid $(NH_4)_2[Ce(NO_3)_6]$ (5.48 g, 10 mmol) was added in portions over a period of 1 h, which resulted in a clear dark solution. The solution was stirred overnight at ambient temperature and then filtered. The filtrate was left undisturbed for several days, during which time a large amount of X-ray quality block crystals of **2** were deposited. The crystals were collected by filtration, washed with water, and dried in air; yield 1.02 g (67% based on Mn). $C_{40}H_{42}CeMn_3N_{15}O_{30}$ (1517.83): calcd. C 31.65, H 2.79, N 13.84; found C 31.74, H 2.87, N 13.75. Selected IR data (KBr): $\tilde{\nu}$ = 3401 (s, br), 1763 (w), 1634 (s), 1603 (s), 1568 (m), 1497 (s), 1448 (s), 138 2 (s), 1306 (s), 1249 (s), 1161 (m), 1124 (w), 1108 (m), 1073 (w), 1057 (w), 1032 (s), 1022 (s), 893 (w), 818 (m), 765 (s), 724 (s), 691 (s), 665 (m), 651 (m), 612 (m), 568 (w), 503 (m), 469 (w), 451 (w), 418 (w) cm^{-1}.

$[Mn_2Ce_3O_6(pta)_6(NO_3)_2(dmf)_4]\cdot H_2O$ (3): Solid $(NH_4)_2[Ce(NO_3)_6]$ (1.64 g, 3.0 mmol) was added in batches to a stirred red solution of $Mn(pta)_2\cdot 2H_2O$ (0.72 g, 2 mmol) in EtOH/dmf (35 mL, v/v 6:1) over a period of 0.5 h, which resulted in a clear brown solution. The solution was stirred at room temperature for 4 h and then filtered. The filtrate was allowed to stand undisturbed for several weeks at room temperature, during which time red-brown amorphous crystalline materials formed. The X-ray quality crystals of **3** were obtained by recrystallizing the amorphous materials with MeCN; yield 0.41 g (22% based on Mn). $C_{60}H_{72}Ce_3Mn_2N_6O_{29}$ (1871.48): calcd. C 38.51, H 3.88, N 4.49; found C 38.62, H 3.83, N 4.40. Selected IR data (KBr): $\tilde{\nu}$ = 3433 (s, br), 1706 (s), 1648 (s), 1610 (s), 1597 (s), 1556 (s), 1524 (s), 1413 (s), 1387 (s), 1292 (m), 1180 (s), 1113 (m), 1021 (m), 961 (w), 847 (m), 764 (s), 693 (m), 623 (s), 567 (s), 503 (w), 471 (m), 408 (w) cm^{-1}.

$[Mn_8CeO_8(pta)_{12}(dmf)_4]$ (4): 4,4′-Bipyridine (0.16 g, 1 mmol) was added to a stirred red solution of $Mn(pta)_2\cdot 2H_2O$ (1.45 g, 4 mmol) in EtOH/dmf (35 mL, v/v 6:1) and then solid $(NH_4)_2[Ce(NO_3)_6]$ (0.55 g, 1 mmol) was added in small portions over a period of 0.5 h. The resulting mixture was stirred at room temperature overnight to yield a dark solution in which a large amount of brown material was suspended. The mixture was filtered and the filtrate was left undisturbed to produce several black crystals that were crystallographically confirmed to be **3**. The solid brown residue was dissolved in a mixture of dmf/dmso/$CHCl_3$ (30 mL, v/v/v 1:1:1) and the insoluble substance was discarded by filtration. The greenish-brown hexagonal column crystals of **4** were formed within one week following natural evaporation of the dark filtrate. The crystals were collected by filtration and dried in air; yield 0.40 g (30% based on Mn). $C_{108}H_{112}CeMn_8N_4O_{36}$ (2621.66): calcd. C 49.48, H 4.31, N 2.14; found C 49.59, H 4.34, N 2.09. Selected IR data (KBr): $\tilde{\nu}$ = 3466 (s, br), 1763 (w), 1648 (s), 1599 (s), 1557 (m), 1529 (s), 1511 (s), 1293 (w), 1256 (w), 1211 (w), 1180 (s), 1150 (w), 1110 (m), 1065 (w), 1040 (w), 1021 (m), 848 (m), 808 (w), 765 (s), 694 (m), 676 (m), 622 (s), 573 (s), 513 (w), 467 (s), 415 (m) cm^{-1}.

X-ray Crystallography: Data for complexes **1** to **4** were collected at 293 K with a Rigaku Mercury CCD area-detector diffractometer

Table 5. The selected crystallographic data and refinement details for complexes **1** to **4**.

	1	**2**	**3**	**4**
Empirical formula	$C_{48}H_{58}Mn_2N_{16}O_{25}$	$C_{40}H_{42}CeMn_3N_{15}O_{30}$	$C_{60}H_{72}Ce_3Mn_2N_6O_{29}$	$C_{108}H_{112}CeMn_8N_4O_{36}$
Formula weight	1368.98	1517.83	1871.48	2621.66
Space group	*P*2/*c*	*Cc*	$P\bar{1}$	$P4_2/n$
a [Å]	13.198(7)	24.816(2)	13.610(3)	20.6466(6)
b [Å]	12.370(6)	15.2835(10)	17.429(3)	20.6466(6)
c [Å]	18.439(10)	17.4941(16)	18.111(4)	17.6530(10)
α [°]	90	90	68.235(7)	90
β [°]	105.821(9)	122.636(3)	71.562(7)	90
γ [°]	90	90	70.043(9)	90
V [Å^3]	2896(3)	5587.4(8)	3660.6(13)	7525.2(5)
Z	2	4	2	2
Absorption coefficient [mm^{-1}]	0.535	1.569	2.247	1.005
F(000)	1416	3040	1860	2668
θ range for data collection [°]	2.30–27.50	2.37–27.48	2.33–27.48	2.29–27.48
Reflections collected/unique (R_{int})	21245/6610 (0.0460)	21434/9628 (0.0471)	28467/16524 (0.0225)	56985/8615 (0.0362)
Data/restraints/parameters	6610/9/414	9628/9/820	16524/1/892	8615/0/354
Goodness-of-fit on F^2	1.007	1.005	1.002	1.002
*R*1/*wR*2 [$I > 2\sigma(I)$]	0.0714/0.2114	0.0513/0.1240	0.0420/0.1053	0.0677/0.1616
*R*1/*wR*2 [all data]	0.0896/0.2358	0.0650/0.1367	0.0554/0.1151	0.0747/0.1641
$(\Delta\sigma)_{max./min.}$ [e Å^{-3}]	0.737/–0.546	0.573/–0.656	1.202/–1.307	0.952/–1.166

with graphite-monochromated Mo-K_α radiation (λ = 0.71073 Å). The data reduction and cell refinement were performed with the CrystalClear program,[25] and the absorption correction was applied by using the SADABS program.[26] The structure was solved by direct methods and subsequent difference Fourier syntheses and was refined on F^2 by full-matrix least-squares methods with the SHELXTL-97 program package.[27] All of the non-hydrogen atoms were refined anisotropically. The aromatic/alkyl hydrogen atoms were introduced in the calculated positions and were treated as riding atoms, while the hydrogen atoms that were bonded on the water molecules in complexes **1** and **2** were located from the difference Fourier syntheses. The water O atoms (O11, O12, and O13) in **1** displayed some disorder, so no effort was made to add H atoms to them. One of the water molecules of crystallization in **3** was disordered and could not be modelled properly, thus the SQUEEZE instruction of the program PLATON was carried out in order to remove its contribution to the overall intensity data.[28] The crystallographic data for **1**–**4** are outlined in Table 5.

CCDC-833032 (for **1**), -833033 (for **2**), -833034 (for **3**), and -833035 (for **4**) contain the supplementary crystallographic data for this paper. These data can be obtained free of charge from The Cambridge Crystallographic Data Centre via www.ccdc.cam.ac.uk/data_request/cif.

Supporting Information (see footnote on the first page of this article): The bond valence sum calculations for the Mn atoms in **1**–**4**, two packing diagrams for **1** and **4**, two tables containing the hydrogen bonds for **1** and **2**, and five tables containing the selected bond angles and/or bond lengths for **1**–**4** are contained in the Supporting Information.

Acknowledgments

This work was supported by the National Natural Science Foundation of China (NSFC) (grant numbers 20973172 and 21071145).

[1] a) T. Lis, *Acta Crystallogr., Sect. B* **1980**, *36*, 2042–2046; b) J. Villain, F. Hartman-Boutron, R. Sessoli, A. Rettori, *Europhys. Lett.* **1994**, *27*, 159–164; c) P. Politi, A. Rettori, F. Hartmann-Boutron, J. Villain, *Phys. Rev. Lett.* **1995**, *75*, 537–540; d) M. Hennion, L. Pardi, I. Mirebeau, E. Suard, R. Sessoli, A. Caneschi, *Phys. Rev. B* **1997**, *56*, 8819–8827; e) A. Caneschi, D. Gatteschi, R. Sessoli, *J. Chem. Soc., Dalton Trans.* **1997**, 3963–3970; f) S. Das, S. Mukhopadhyay, *Eur. J. Inorg. Chem.* **2007**, 4500–4507; g) V. L. Pecoraro, W. Y. Hsieh, *Inorg. Chem.* **2008**, *47*, 1765–1778.

[2] a) R. Manchanda, G. W. Brudvig, R. H. Crabtree, *Coord. Chem. Rev.* **1995**, *144*, 1–38; b) V. K. Yachandra, K. Sauer, M. P. Klein, *Chem. Rev.* **1996**, *96*, 2927–2950; c) W. Ruttinger, G. C. Dismukes, *Chem. Rev.* **1997**, *97*, 1–24; d) S. Mukhopadhyay, S. K. Mandal, S. Bhaduri, W. H. Armstrong, *Chem. Rev.* **2004**, *104*, 3981–4026; e) J. Messinger, J. Yano, J. Kern, K. Sauer, M. J. Latimer, Y. Pushkar, J. Biesiadka, B. Loll, W. Saenger, A. Zouni, V. K. Yachandra, *Science* **2006**, *314*, 821–825; f) Y. Umena, K. Kawakami, J.-R. Shen, N. Kamiya, *Nature* **2011**, *473*, 55–60.

[3] a) G. Christou, *Acc. Chem. Res.* **1989**, *22*, 328–335; b) R. J. Debus, *Biochem. Biophys. Acta* **1992**, *1102*, 269–352; c) V. K. Yachandra, V. J. Derose, M. J. Latimer, I. Mukerji, K. Sauer, M. P. Klein, *Science* **1993**, *260*, 675–679; d) K. Wieghardt, *Angew. Chem.* **1994**, *106*, 765; *Angew. Chem. Int. Ed. Engl.* **1994**, *33*, 725–729; e) V. L. Pecoraro, M. J. Baldwin, A. Gelasco, *Chem. Rev.* **1994**, *94*, 807–826; f) O. Horner, M. F. Charlot, A. Boussac, E. Anxolabehere-Mallart, L. Tchertanov, J. Guilhem, J. J. Girerd, *Eur. J. Inorg. Chem.* **1998**, 721–727; g) M. Yagi, M. Kaneko, *Chem. Rev.* **2001**, *101*, 21–35; h) J. Yano, K. Sauer, J. J. Girerd, V. K. Yachandra, *J. Am. Chem. Soc.* **2004**, *126*, 7486–7495; i) K. Sauer, J. Yano, V. K. Yachandra, *Coord. Chem. Rev.* **2008**, *252*, 318–335; j) C. S. Mullins, V. L. Pecoraro, *Coord. Chem. Rev.* **2008**, *252*, 416–443; k) G. C. Dismukes, R. Brimblecombe, G. A. N. Felton, R. S. Pryadun, J. E. Sheats, L. Spiccia, G. F. Swiegers, *Acc. Chem. Res.* **2009**, *42*, 1935–1943; l) A. R. Jaszewski, R. Stranger, R. J. Pace, *J. Phys. Chem. B* **2011**, *115*, 4484–4499.

[4] a) A. M. Ako, I. J. Hewitt, V. Mereacre, R. Clerac, W. Wernsdorfer, C. E. Anson, A. K. Powell, *Angew. Chem.* **2006**, *118*, 5048; *Angew. Chem. Int. Ed.* **2006**, *45*, 4926–4929; b) A. J. Tasiopoulos, S. P. Perlepes, *Dalton Trans.* **2008**, 5537–5555; c) C.-H. Ge, Z.-H. Ni, C.-M. Liu, A.-L. Cui, D.-Q. Zhang, H.-Z. Kou, *Inorg. Chem. Commun.* **2008**, *11*, 675–677; d) E. E. Moushi, T. C. Stamatatos, W. Wernsdorfer, V. Nastopoulos, G. Christou, A. J. Tasiopoulos, *Inorg. Chem.* **2009**, *48*, 5049–5051.

[5] a) R. Sessoli, H.-L. Ysai, A. R. Schake, S. Wang, J. B. Vincent, K. Folting, D. Gatteschi, G. Christou, D. N. Hendrickson, *J. Am. Chem. Soc.* **1993**, *115*, 1804–1816; b) R. Sessoli, D. Gatteschi, A. Caneschi, M. A. Novak, *Nature* **1993**, *365*, 141–143; c) M. Soler, S. K. Chandra, E. R. Davidson, G. Christou, D. Ruiz, D. N. Hendrickson, *Chem. Commun.* **2000**, 2417–2418; d) W. Wernsdorfer, N. Aliaga-Alcalde, D. N. Hendrickson, G. Christou, *Nature* **2002**, *416*, 406–409; e) D. J. Price, S. R. Batten, B. Moubaraki, K. S. Murray, *Chem. Commun.* **2002**, 762–763; f) W. Wernsdorfer, M. Soler, G. Christou, D. N. Hendrickson, *J. Appl. Phys.* **2002**, *91*, 7164–7166; g) M. Soler, W. Wernsdorfer, K. A. Abboud, J. C. Huffman, E. R. Davidson, D. N. Hendrickson, G. Christou, *J. Am. Chem. Soc.* **2003**, *125*, 3576–3588; h) G. Christou, *Polyhedron* **2005**, *24*, 2065–2075.

[6] a) D. Loss, D. P. Divincenzo, G. Grinstein, D. D. Awschalom, J. F. Smyth, *Physica. B* **1993**, *189*, 189–203; b) S. M. J. Aubin, M. W. Wemple, D. M. Adams, H. L. Tsai, G. Christou, D. N. Hendrickson, *J. Am. Chem. Soc.* **1996**, *118*, 7746–7754; c) L. Thomas, F. Lionti, R. Ballou, D. Gatteschi, R. Sessoli, B. Barbara, *Nature* **1996**, *383*, 145–147; d) C. Dendrinou-Samara, M. Alexiou, C. M. Zaleski, J. W. Kampf, M. L. Kirk, D. P. Kessissoglou, V. L. Pecoraro, *Angew. Chem.* **2003**, *115*, 3893; *Angew. Chem. Int. Ed.* **2003**, *42*, 3763–3766; e) C. J. Milios, C. P. Raptopoulou, A. Terzis, F. Lloret, R. Vicente, S. P. Perlepes, A. Escuer, *Angew. Chem.* **2004**, *116*, 212; *Angew. Chem. Int. Ed.* **2004**, *43*, 210–212; f) H. Miyasaka, R. Clerac, W. Wernsdorfer, L. Lecren, C. Bonhomme, K. Sugiura, M. Yamashita, *Angew. Chem.* **2004**, *116*, 2861; *Angew. Chem. Int. Ed.* **2004**, *43*, 2801–2805; g) A. K. Boudalis, B. Donnadieu, V. Nastopoulos, J. M. Clemente-Juan, A. Mari, Y. Sanakis, J. P. Tuchagues, S. P. Perlepes, *Angew. Chem.* **2004**, *116*, 2316; *Angew. Chem. Int. Ed.* **2004**, *43*, 2266–2270; h) H. Oshio, N. Hoshino, T. Ito, M. Nakano, *J. Am. Chem. Soc.* **2004**, *126*, 8805–8812; i) A. Cornia, A. F. Costantino, L. Zobbi, A. Caneschi, D. Gatteschi, M. Mannini, R. Sessoli, *Structure and Bonding* **2006**, *122*, 133–161; j) C.-B. Ma, M.-Q. Hu, H. Chen, C.-N. Chen, Q.-T. Liu, *Eur. J. Inorg. Chem.* **2008**, 5274–5280.

[7] a) S. Menege, M. N. Collomb-Dunand-Sauthier, C. Lambeaux, M. Fontecave, *J. Chem. Soc., Chem. Commun.* **1994**, 1885–1886; b) H. Cao, S. L. Suib, *J. Am. Chem. Soc.* **1994**, *116*, 5334–5342; c) A. Trovarelli, *Catal. Rev. Sci. Eng.* **1996**, *38*, 439–509; d) D. Duprez, F. Delanoë, J. Barbier **Jr**, P. Isnard, G. Blanchard, *Catal. Today* **1996**, *29*, 317–322; e) Z. Y. Ding, L. Li, D. Wade, E. F. Gloyna, *Ind. Eng. Chem. Res.* **1998**, *37*, 1707–1716; f) S. Aki, M. A. Abraham, *Ind. Eng. Chem. Res.* **1999**, *38*, 358–367; g) Q. Feng, H. Kanoh, K. Ooi, *J. Mater. Chem.* **1999**, *9*, 319–333; h) S. Hamoudi, K. Belkacemi, A. Sayari, F. Larachi, *Chem. Eng. Sci.* **2001**, *56*, 1275–1281; i) C.-M. Hung, J.-C. Lou, C.-H. Lin, *Environ. Eng. Sci.* **2003**, *20*, 547–556; j) M. Abecassis-Wolfovich, M. V. Landau, A. Brenner, M. Herskowitz, *Ind. Eng. Chem. Res.* **2004**, *43*, 5089–5097; k) F. Arena, J. Negro, A. Parmaliana, L. Spadaro, G. Trunfio, *Ind. Eng. Chem. Res.* **2007**, *46*, 6724–6731; l) R. Levi, M. Milman, M. V. Lan-

dau, A. Brenner, M. Herskowitz, *Environ. Sci. Technol.* **2008**, *42*, 5165–5170.
[8] a) A. J. Tasiopoulos, T. A. O'Brien, K. A. Abboud, G. Christou, *Angew. Chem.* **2004**, *116*, 349; *Angew. Chem. Int. Ed.* **2004**, *43*, 345–349; b) M. Murugesu, A. Mishra, W. Wernsdorfer, K. A. Abboud, G. Christou, *Polyhedron* **2006**, *25*, 613–625; c) A. J. Tasiopoulos, A. Mishra, G. Christou, *Polyhedron* **2007**, *26*, 2183–2188; d) C. J. Milios, P. A. Wood, S. Parsons, D. Foguet-Albiol, C. Lampropoulos, G. Christou, S. P. Perlepes, E. K. Brechin, *Inorg. Chim. Acta* **2007**, *360*, 3932–3940.
[9] a) H.-S. Wang, C.-B. Ma, M. Wang, C.-N. Chen, Q.-T. Liu, *J. Mol. Struct.* **2008**, *875*, 288–294; b) M. Wang, D.-Q. Yuan, C.-B. Ma, M.-J. Yuan, M.-Q. Hu, N. Li, H. Chen, C.-N. Chen, C. N. Q.-T. Liu, *Dalton Trans.* **2010**, *39*, 7276–7285.
[10] G. V. Romanenko, E. Y. Fursova, V. I. Ovcharenko, *Russ. Chem. Bull.* **2009**, *58*, 1–10.
[11] V. Mereacre, A. M. Ako, M. N. Akhtar, A. Lindemann, C. E. Anson, A. K. Powell, *Helv. Chim. Acta* **2009**, *92*, 2507–2524.
[12] a) K. R. Reddy, M. V. Rajasekharan, *Polyhedron* **1994**, *13*, 765–769; b) K. R. Reddy, M. V. Rajasekharan, N. Arulsamy, D. J. Hodgson, *Inorg. Chem.* **1996**, *35*, 2283–2286.
[13] a) J. E. Sarneski, H. H. Thorp, G. W. Brudvig, R. H. Crabtree, G. K. Schulte, *J. Am. Chem. Soc.* **1990**, *112*, 7255–7260; b) C. Philouze, G. Blondin, J.-J. Girerd, J. Guilhem, C. Pascard, D. Lexa, *J. Am. Chem. Soc.* **1994**, *116*, 8557–8565; c) J. Limburg, J. S. Vrettos, L. M. Liable-Sands, A. L. Rheingold, R. H. Crabtree, G. W. Brudvig, *Science* **1999**, *283*, 1524–1527; d) S. Mukhopadhyay, W. H. Armstrong, *J. Am. Chem. Soc.* **2003**, *125*, 13010–13011; e) H. Chen, J. W. Faller, R. H. Crabtree, G. W. Brudvig, *J. Am. Chem. Soc.* **2004**, *126*, 7345–7349; f) M.-N. Collomb, A. Deronzier, A. Richardot, J. Pecaut, *New J. Chem.* **1999**, *23*, 351–353; g) H. Chen, M.-N. Collomb, C. Duboc, G. Blondin, E. Riviere, J. W. Faller, R. H. Crabtree, G. W. Brudvig, *Inorg. Chem.* **2005**, *44*, 9567–9573; h) C. Baffert, M.-N. Collomb, A. Deronzier, J. Pecaut, J. Limburg, R. H. Crabtree, G. W. Brudvig, *Inorg. Chem.* **2002**, *41*, 1404–1400; i) B. C. Dave, R. S. Czernuszewicz, *New J. Chem.* **1994**, *18*, 149–155; j) A. J. Tasiopoulos, K. A. Abboud, G. Christou, *Chem. Commun.* **2003**, 580–581; k) S. Mukhopadhyay, R. J. Staples, W. H. Armstrong, *Chem. Commun.* **2002**, 864–865; l) H. Chen, R. Tagore, S. Das, C. Incarvito, J. W. Faller, R. H. Crabtree, G. W. Brudvig, *Inorg. Chem.* **2005**, *44*, 7661–7670.
[14] a) M. Stebler, A. Ludi, H.-B. Burgi, *Inorg. Chem.* **1986**, *25*, 4743–4750; b) D. Huang, W. Wang, X. Zhang, C. Chen, F. Chen, Q. Liu, D. Liao, L. Li, L. Sun, *Eur. J. Inorg. Chem.* **2004**, 1454–1464.
[15] N. Auger, J.-J. Girerd, M. Corbella, A. Gleizes, J.-L. Zimmermann, *J. Am. Chem. Soc.* **1990**, *112*, 448–450.
[16] a) R. Tagore, R. H. Crabtree, G. W. Brudvig, *Inorg. Chem.* **2007**, *46*, 2193–2203; b) D. Lieb, A. Zahl, T. E. Shubina, I. Ivanovic-Burmazovic, *J. Am. Chem. Soc.* **2010**, *132*, 7282–7284; c) E. M. Sproviero, J. A. Gascón, J. P. McEvoy, G. W. Brudvig, V. S. Batista, *J. Am. Chem. Soc.* **2008**, *130*, 3428–3442.
[17] J. K. Hurst, *Coord. Chem. Rev.* **2005**, *249*, 313–328.
[18] C. Kollmar, M. Couty, O. Kahn, *J. Am. Chem. Soc.* **1991**, *113*, 7994–8005.
[19] C. J. O'Connor, *Prog. Inorg. Chem.* **1982**, *29*, 203–283.
[20] N. A. Law, J. W. Kampf, V. L. Pecoraro, *Inorg. Chim. Acta* **2000**, *297*, 252–264, and references cited therein.
[21] O. Kahn, *Molecular Magnetism*, VCH, Weinheim, Germany, **1993**.
[22] D. Nowak, E. Woźnicka, A. Kuźniar, M. Kopacz, *J. Alloys Compd.* **2006**, *425*, 59–63.
[23] M. P. Shores, J. J. Sokol, J. R. Long, *J. Am. Chem. Soc.* **2002**, *124*, 2279–2292.
[24] A. Mishra, A. J. Tasiopoulos, W. Wernsdorfer, E. E. Moushi, B. Moulton, M. J. Zaworotko, K. A. Abboud, G. Christou, *Inorg. Chem.* **2008**, *47*, 4832–4843.
[25] *CrystalClear*, v.1.3.6. Rigaku/MSC, The Woodlands, Texas, USA, **2004**.
[26] G. M. Sheldrick, *SADABS*, *Siemens Area Detector Absorption Correction Program*, v.2.01, Bruker AXS, Madison, WI, USA, **1998**.
[27] G. M. Sheldrick, *SHELXL-97*, *Program for the Refinement of Crystal Structure*, University of Göttingen, Germany, **1997**.
[28] A. L. Spek, *Acta Crystallogr., Sect. D* **2009**, *65*, 148–155.

Received: July 12, 2011
Published Online: October 10, 2011

